JOURNAL OF MATERIALS SCIENCE 21 (1986) 2033–2042

Dependence of oxidation rate of WC powder on particle size

B. ROEBUCK, E.G. BENNETT, E. A. ALMOND, M. G. GEE
National Physical Laboratory, Teddington, Middlesex TW11 0LW, UK

Isothermal oxidation experiments on WC powders revealed a systematic dependence of oxidation rate on powder particle size. Oxidation was followed by measuring the change in mass of the WC powder as WC is converted to WO_3. Fine powders oxidized more quickly than coarse powders because for the same initial mass the fine powder had a larger surface area. Measurement of the change in mass with time were shown to resolve differences in mean size of 0.1 μm, and possibly less, between separate batches of powder. A theoretical expression for the change in mass with time of spherical particles has been derived which compares well with experimental measurements and which can also be used with appropriate assumptions to calculate the initial powder-size distribution.

1. Introduction

Although there have been several studies [1–5] of the oxidation of loose powder samples of WC, few investigations have been made of the dependence of oxidation rate on physical characteristics. It has been found that the kinetics of oxidation are usually determined by the type of oxide film that is formed and that the production of gaseous reaction products, such as CO and CO_2, leads to rupture of the oxide layer. Ingress of oxygen through cracks and pores enables oxidation to proceed rapidly.

Linear oxidation rates have been measured on hot-pressed compacts of WC powders at 700° C [5] with a rate constant of $4 \times 10^{-2}\,g\,m^{-2}\,sec^{-1}$ and on WC powder between 500 and 650° C [1]. The latter study provided an activation energy of $188\,kJ\,mol^{-1}$ for the reaction, microcracks were detected in the WO_3 film, and non-linear oxidation rates were obtained when there was an increase in temperature or in the partial pressure of O_2. Linear oxidation rates have also been observed in studies of WC/Co cemented carbides [2–4], and the reaction rate constants [3] over a range of temperatures were similar to the value obtained for hot-pressed powders.

The chemical reaction during linear oxidation is

$$2WC + 5O_2 \rightarrow 2WO_3 + 2CO_2$$

and since the controlling factor is the availability of fresh surface area of WC, it is reasonable to predict that WC powder samples of equal mass but different particle sizes will oxidize at different rates.

The hypothesis was examined by studying the oxidation kinetics of several different WC powders, over the temperature range 400 to 600° C, in a thermogravimetric analyser. Preliminary experiments showed that the hypothesis was probably correct, particularly at low oxidizing temperatures, that is less than 500° C, since the change of mass with time was markedly different for each powder. In addition, the total change in mass was that to be expected for converting WC to WO_3 on the basis of relative atomic weights.

The success of the preliminary experiments allowed two broad objectives to be defined:

(a) to examine the experimental uncertainties associated with the oxidation of WC powders, and to ascribe limits to the predictability of the reaction;

(b) to develop a simple theoretical analysis for estimating particle size from the change in mass with time as the powder oxidizes.

For this purpose it was decided to study the oxidation kinetics of three WC powders with particle sizes that spanned the range of materials in present use for manufacturing hardmetals. The nominal sizes chosen were ultrafine (UF), fine (F) and coarse (C) with approximate particle diameters of 0.5, 1 and 6 μm, respectively.

2. Materials and experiments

Details of the powders used are given in Table I. Values for the average particle diameters were obtained by examining the powders by scanning electron microscopy. Micrographs of the powders are shown in Fig. 1.

The isothermal oxidation experiments were performed in equipment for thermogravimetric analysis (TGA). A weighed sample, 319 ± 1 mg, of powder was placed in a small platinum crucible. The crucible was put on the end of an alumina rod connected to the lever arm of a sensitive balance. The preheated furnace was then lowered over the crucible. As the powder oxidized the change in mass was converted into a displacement by the movement of a lever arm on a pen recorder with a constant chart speed, to give a graph of mass against time for each powder. A 1 mm deflection on the chart was equivalent to a change in mass of 1 mg. The experiments were carried out at temperatures between 400 and 550° C. Tests at

0022–2461/86 $03.00 + .12

TABLE I Properties of the WC powders

Powder	Average particle diameter*, d_E (μm)	FSSS† (μm)	Total carbon‡ (wt %)	Free carbon‡ (wt %)
Ultrafine (UF)	0.30	0.80	6.14	0.04
Fine (F)	1.15	1.72	6.18	0.07
Coarse (C)	6.50	7.05	6.18	0.07

*Obtained from scanning electron micrographs.
†Fisher sub-sieve size.
‡Details provided by powder suppliers (Lederman Gmbh, Horb am Neckar, FRG, for UF; Wimet Ltd, UK, for F and C).

temperatures below 400° C were inconviently slow, whereas at temperatures greater than about 550° C the oxidation reaction appeared to be too fast for the response time of the equipment.

A thermocouple placed inside the furnace tube was used to record the indicated temperature, T_i, of the TGA equipment during an experiment. The same thermocouple served to control the furnace temperature. On the chart, a displacement of about 1 mm was equivalent to a temperature interval of about 10° C. Consequently, temperature reproducibility for experiments run at different times was not better than about $\pm 3°$ C. In a calibration experiment the temperature of the powder, T_p, was checked by placing another thermocouple directly into the powder. It was found that

$$T_p = T_i + 0.05(600 - T_i) \quad (1)$$

and thus, especially at low temperatures, the powder was at a higher temperature than was indicated by the furnace thermocouple. The calibration experiment also showed that the limits of furnace control were about $\pm 2°$ C.

Some of the oxidation experiments were performed at different temperatures in order to obtain an activation energy, Q, for the oxidation process from the application of the equation

$$\alpha = \alpha_0 \exp(-Q/RT) \quad (2)$$

where α is the reaction rate constant, α_0 is a pre-exponential factor, T is the temperature and R is the gas constant.

3. Theory

As a result of oxidation, a mass, M_0, of WC increases with time as the WC is converted to WO_3. The final mass of WO_3 is BM_0 where B is a constant. The value of B is 1.183 and is obtained by taking a ratio of the atomic weights of WO_3 to WC, A_{WO_3}/A_{WC}. It is known [1–5] that the oxidation of WC is a linear process, probably because the WO_3 does not form a coherent protective layer. Therefore in order to obtain an expression for the change in mass with time, dM/dt, it is assumed that the molecular conversion process results in a reaction rate which is controlled by the surface area of WC at a given time t. Thus it follows that the radius, r, of a given particle of WC decreases linearly with time. Thus

$$dr/dt = -\alpha \quad (3)$$

where α is a constant with dimensions of LT^{-1}. Therefore

$$r = r_0 - \alpha t \quad (4)$$

where r_0 is the initial particle radius.

The initial mass, M_I, of a batch of WC powder in which the number distribution density of spherical particles is $N(r_i)$ is given by

$$M_I = \int_0^\infty \tfrac{4}{3}\pi\varrho r_i^3 N(r_i)\, dr_i \quad (5)$$

Therefore the mass of WC, M_t, remaining after time

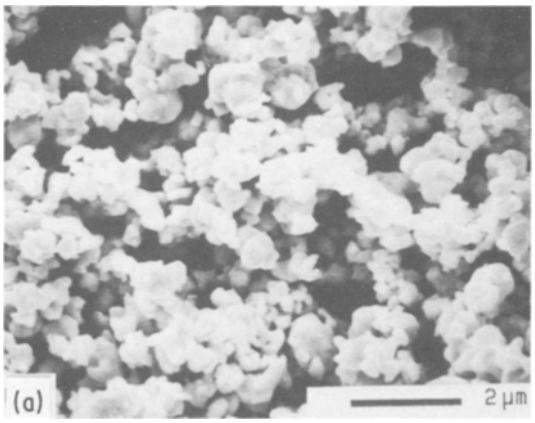

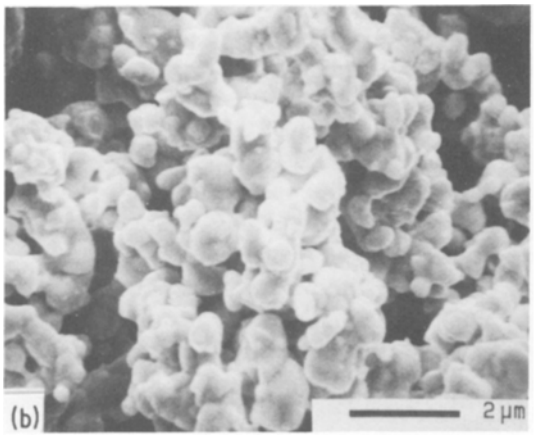

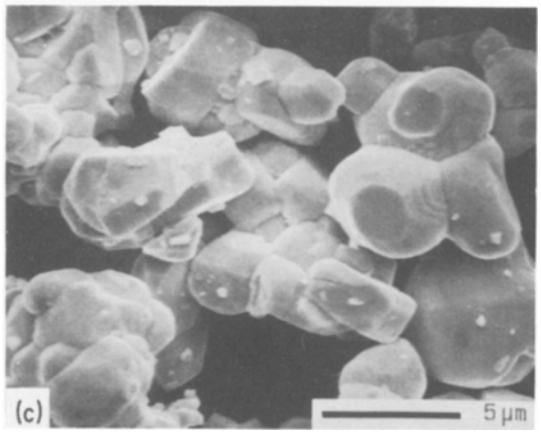

Figure 1 Scanning electron micrographs of the three WC powders: (a) UF, (b) F, (c) C.

t of oxidation is given by

$$\frac{M_t}{M_1} = \frac{\int_{\alpha t}^{\infty} (r_i - \alpha t)^3 N(r_i)\, dr_i}{\int_0^{\infty} r_i^3 N(r_i)\, dr_i} \quad (6)$$

The integration limits are between αt and infinity to take account of the fact that particles with sizes smaller than αt are completely oxidized after time t. Thus the change in mass with time of a batch of WC powder is uniquely defined for a given form of $N(r_i)$, and Equation 6 can be evaluated by making an assumption about the form taken by $N(r_i)$. The theoretical variation of M_t/M_1 can then be iteratively compared with the experimentally measured change in order to achieve a good estimate for $N(r_i)$. Three examples of simple distributions serve to illustrate the application of the analysis.

First, for particles of single size, Equation 6 takes the simple form

$$\frac{M_t}{M_1} = \frac{(r_0 - \alpha t)^3}{r_0^3} \qquad \alpha t \leqslant r_0 \quad (7)$$

For particles with mixed fractions of particles of single size

$$\frac{M_t}{M_1} = \frac{\sum_i N_i'(r_i - \alpha t)^3}{\sum_i N_i' r_i^3} \quad (8)$$

for i fraction populations, N_i', of initial radii r_i.

However, in practice the distribution of particle sizes within a batch is probably log–normal in form and in this case Equation 6 takes the following form (see Appendix):

$$\frac{M_t}{M_1} = \int_{\alpha t}^{\infty} (r_i - \alpha t)^3 \frac{N}{(2\pi\sigma^2)^{1/2}} \frac{1}{r_i} \times \exp\left(-\frac{(\ln r_i - m)^2}{2\sigma^2}\right) dr_i \left[\int_0^{\infty} r_i^3 \frac{N}{(2\pi\sigma^2)^{1/2}} \frac{1}{r_i} \times \exp\left(-\frac{(\ln r_i - m)^2}{2\sigma^2}\right) dr_i\right]^{-1} \quad (9)$$

where N is the total, m is the mean and σ is the standard deviation of $\ln r_i$. Equation 9 can be evaluated numerically by making a number of assumptions (see Appendix).

Equations 6 to 9 define the change in mass of WC with time. However, the measured change in mass comprises the loss in mass of WC plus the gain in mass of WO_3. The total mass of oxide and carbide, M_t', at a given time t is thus

$$M_t' = M_t + B(M_1 - M_t) = BM_1 + (1 - B)M_t \quad (10)$$

and therefore

$$\frac{M_t'}{M_1} = B + \frac{M_t}{M_1}(1 - B) \quad (11)$$

Therefore the total mass change of oxide and carbide is linearly related to the change in mass with time of the remaining unoxidized WC and, for single-sized particles,

$$\frac{M_t'}{M_1} = B + (1 - B)\frac{(r_0 - \alpha t)^3}{r_0^3} \quad (12)$$

The above analysis indicates that WC particles of different initial radius will gain in mass at different rates during oxidation. Thus a measurement of mass change with time of a batch of WC powder of unknown particle size will allow r_0 to be calculated if a value for the constant α is known.

4. Results and discussion

In assessing and comparing the results of the oxidation experiments with theory, the change in mass has been expressed as starting from a value of unity (equivalent to the start of the reaction) and finishing at a value of zero (equivalent to the end of the reaction when all the WC had been converted to WO_3). In practice, the mass increased by a factor of 1.183 (A_{WO_3}/A_{WC}). For all the experiments the change in mass (about 58.5 mg) was equal to that expected for complete conversion of WC to WO_3 within the uncertainty in reading change in mass from the recorder, which was about 0.5 mg (about 1% of the total change).

4.1. Comparison with theory for single-sized particles

The theoretical analysis for single-sized particles indicated that the change in mass with time could be

TABLE II Cubic regression analysis of changes in mass

Specimen	Isothermal oxidation temperature (indicated, T_i)	Regression coefficient, R^2	α/r (min^{-1}) from Equation 13			
			Coefficient of t	Coefficient of t^2	Coefficient of t^3	Average
UF	390	0.998	0.001 20	0.001 18	0.001 18	0.001 19
	440	0.998	0.003 23	0.003 16	0.003 15	0.003 18
	440	0.999	0.003 02	0.003 03	0.003 03	0.003 03
F	440	0.998	0.000 875	0.000 845	0.000 828	0.000 849
	440	0.997	0.001 12	0.001 09	0.001 08	0.001 09
	470	0.998	0.002 21	0.002 13	0.002 07	0.002 14
	500	0.998	0.005 48	0.005 40	0.005 37	0.005 41
	500	0.999	0.005 60	0.005 63	0.005 63	0.005 62
C	440	0.999	0.000 155	0.000 155	0.000 157	0.000 156
	500	1.000	0.000 882	0.000 902	0.000 917	0.000 9
	540	1.000	0.001 72	0.001 78	0.001 83	0.001 78
	580	0.993	0.004 72	0.004 89	0.004 90	0.004 84

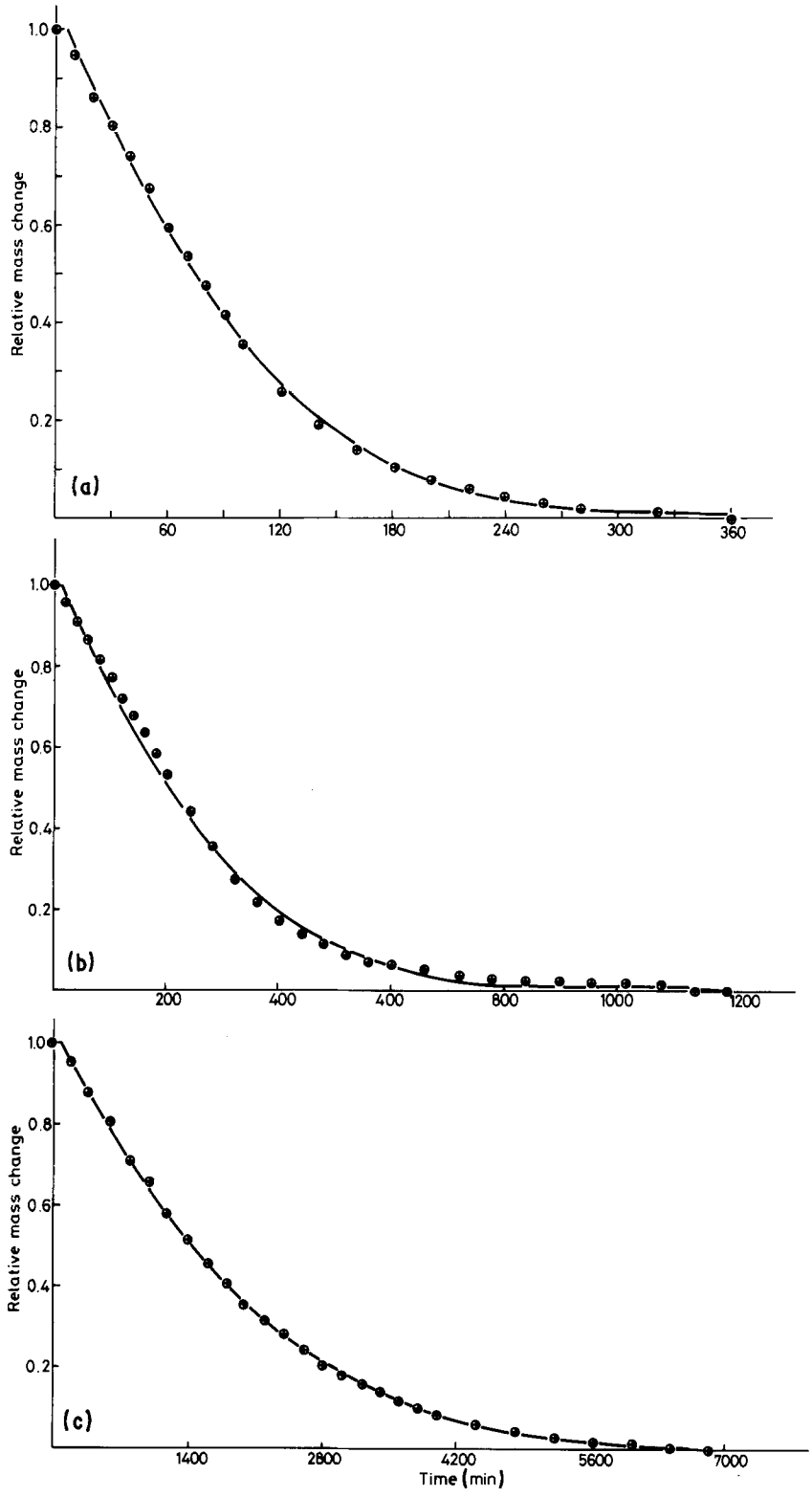

Figure 2 Mass changes during oxidation at 440° C, compared with theory (single-sized particles): (a) UF, (b) F, (c) C. Solid lines represent theory (cubic fit).

expressed as

$$\frac{M_t}{M_I} = \frac{(r_0 - \alpha t)^3}{r_0^3}$$

or

$$\frac{M'_t}{M_I} = B + (1 - B)\frac{(r_0 - \alpha t)^3}{r_0^3}$$

and

$$\frac{(r_0 - \alpha t)^3}{r_0^3} = 1 - 3\left(\frac{\alpha}{r_0}\right)t + 3\left(\frac{\alpha}{r_0}\right)^2 t^2 - \left(\frac{\alpha}{r_0}\right)^3 t^3 \quad (13)$$

To assess the accuracy of the theoretical expression a regression analysis was performed on the experimental data for change in mass with time for about 20 to 30 individual points taken from the chart record. The results of the analysis are shown in Table II for all the experiments, and in Fig. 2 for plots of change in mass with time at an indicated furnace temperature of 440° C for each of the powders. Some tests were repeated to check reproducibility. The results in Table II and Fig. 2 indicate that the agreement between theory and experiment was very close, with regression coefficients (R^2) close to a value of unity. Added confirmation came from the close similarity between the values for α/r determined from each of the coefficients of t, t^2 and t^3.

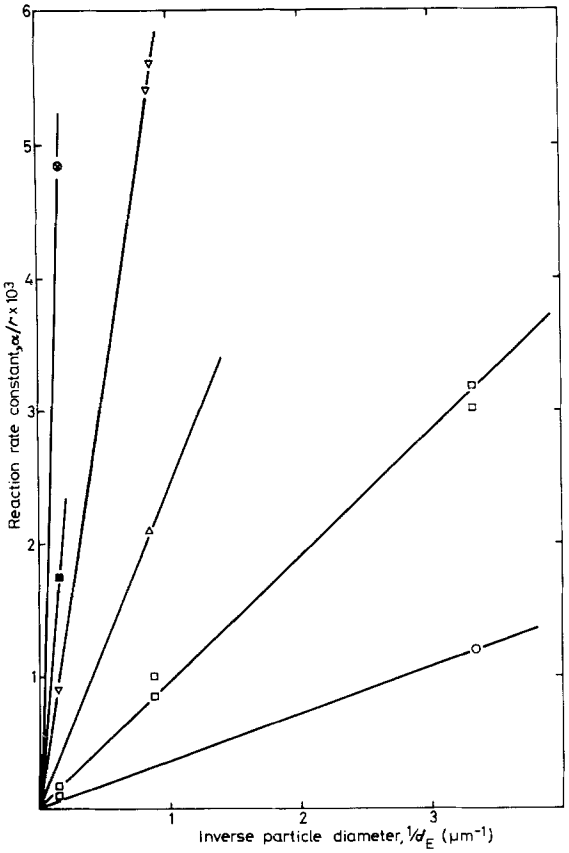

Figure 3 Reaction rate constants, α/r, against inverse particle diameter at various temperatures: (○) 390° C, (□) 440° C, (△) 470° C, (▽) 500° C, (■) 540° C, (⊗) 580° C.

It is evident from Equation 13 that only values of α/r could be obtained from the comparison of theory with experiment. In order to obtain a value for α at each temperature an independent measure of r is needed which would subsequently enable r values for other powders to be obtained.

In separate experiments each of the powders was sized by image analysis of scanning electron micrographs and the results are given in Table I. There are uncertainties in measuring particle size by image analysis because of the difficulties in differentiating between particles, grains and agglomerates. However, a plot of α/r against $1/d_E$, where d_E is the particle size obtained by image analysis, is shown in Fig. 3. A reasonably linear correlation was obtained for measurements at temperatures of 440 and 500° C. Thus straight lines have been drawn through the data obtained at other temperatures and the origin, even though there were a limited number of measurements at some temperatures. The slope of the lines thus provides a measure of α at each temperature calculated using Equation 1, which can then be used to obtain an activation energy.

TABLE III Activation energy results from particle size data

α_s, slope of α/r against $1/d_E$	Powder temperature*, T_p (° C)
0.000 34	401
0.001 00	448
0.002 50	477
0.006 40	505
0.011 10	543
0.030 00	581

*Corrected from indicated temperature using Equation 1.

4.2. Activation energy for oxidation

An activation energy for oxidation can be obtained in two ways. In the first, the values of α obtained from Fig. 3, α_s, can be plotted against temperature as $\ln \alpha_s$ against $1/T$ (K^{-1}). These data are given in Table III and shown in Fig. 4. The data fit well to the equation

$$\alpha = \alpha_0 \exp(-Q/RT) \quad (14)$$

with values of 124 kJ mol^{-1} for Q and 9.5×10^5 $\mu m\ min^{-1}$ for α_0.

In the second method, the values of α/r obtained for each of the powders can be also plotted against temperature as $\ln \alpha/r$ against $1/T$. The data are given in

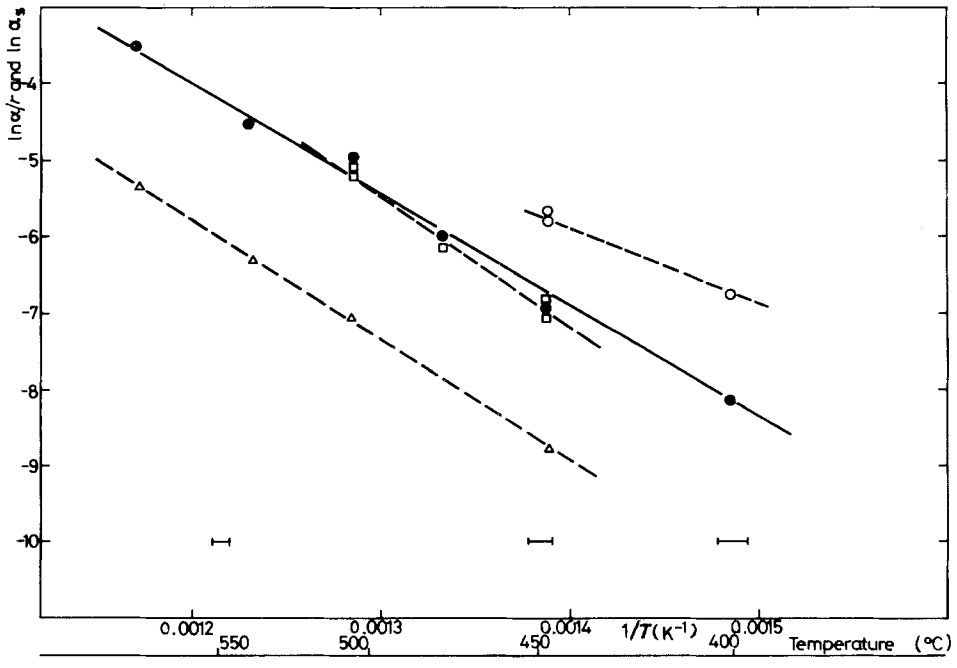

Figure 4 Activation energy plot (log of reaction rate constant, α/r, and $\ln \alpha_s$, against inverse temperature): (○) UF, (□) F, (△) C, (●) combined. Bars represent uncertainty of ± 3° C in temperature.

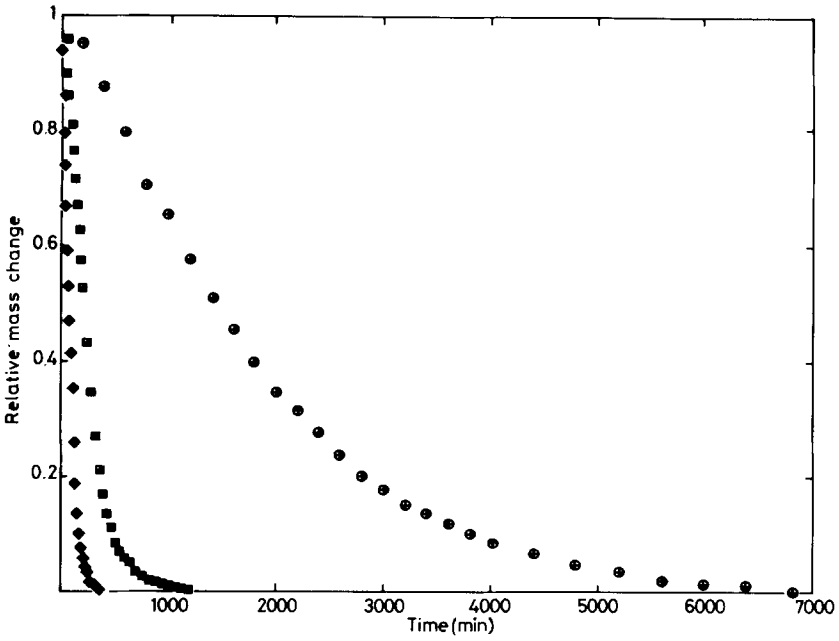

Figure 5 Experimentally measured changes in mass during oxidation at 440° C for the three WC powders: (◆) UF, (■) F, (●) C.

Table II and shown in Fig. 4. The results obtained from the F and C powders are consistent with each other and with the results plotted as ln α_s against $1/T$. The values for α_0/r and Q were 1.8×10^7 and 4×10^5 min^{-1} and 143 and 131 kJ mol^{-1}, respectively, for the F and C powders. The data from the UF powders did not agree equally well and this is possibly due to a combination of a limited number of results and a greater uncertainty in the true temperature of the experiment, performed at an indicated temperature of 390° C. The values for activation energy for oxidation differ from previous work [1] in which a value of 188 kJ mol^{-1} was obtained. However, the latter experiments were performed in relatively low O_2 partial pressures.

4.3. Particle-size differentiation

Having shown that the change in mass with time can be closely fitted to a cubic expression, the question arises as to what are the limiting factors which determine whether oxidation rate can be deduced from particle size or vice versa. For the three powders examined in the present work the differences between the oxidation rates were large (Fig. 5) and there were no difficulties in discrimination.

However, in order to examine this factor more carefully, computer-generated curves of Equation 13 were produced with the value of α set arbitrarily at 0.0005 μm min^{-1} and with values of r between 0.1 to 1 μm at 0.1 μm intervals. The curves are shown in Fig. 6a, which indicates that provided the correct temperature is chosen it ought to be possible to resolve 0.1 μm steps in powder size with little difficulty. However, Fig. 6 was drawn with a fixed value of α of 0.0005 μm min^{-1}. In practice, an uncertainty in α, which arises from its dependence on temperature, requires that a more realistic way of drawing the curves in Fig. 6a would include appropriate error bars. However, for simplicity and to emphasize the potential of the method for size discrimination, this has been shown schematically in Fig. 6b for one curve with a value of r set at 0.65 μm. Two error bands are shown, one for $\pm 2°$ C and the other for $\pm 3°$ C. The uncertainty of $\pm 2°$ C corresponds to that from temperature control. The uncertainty $\pm 3°$ C corresponds to that from reading the indicated temperature from the chart recorder.

Fig. 6 indicates that with the present apparatus a resolution of 0.1 μm between different batches of powder is only just attainable. However, with better temperature control, which is available on more modern TGA equipment, it should be possible to resolve even smaller differences.

4.4. Mixed particle-size distributions

The good agreement between the theory for single-sized particles and experiment indicates that the method could equally be used for analysing mixtures of particles, since Equation 6 can be modified to take account of mixed sizes. For example, for a powder mixture comprising particles of sizes r_i, where n_i are the number fractions of the particle sizes, then

$$\frac{M_t}{M_I} = \frac{\Sigma\, n_i (r_i - \alpha t)^3}{\Sigma\, n_i r_i^3} \tag{15}$$

and M_t/M_I can easily be computed as a function of time, t, provided that for each value of i the summation for that particular term is stopped once $\alpha t \geqslant r_i$. The values of n_i are calculated from m_i, the individual mass fractions, as

$$n_i = \frac{m_i/r_i^3}{\Sigma\, m_i/r_i^3} \tag{16}$$

To illustrate Equation 15 a plot has been drawn (Fig. 7a) of the relative change in mass for a mixture of two powders with values of r_1 and r_2 set at 1 and 0.25 μm, and m_1 equal to 1.0, 0.8, 0.5, 0.2 and 0. The rate constant was arbitrarily chosen to be 0.0005 μm min^{-1}.

Equation 15 can also be used to examine the possibility of detecting a small number of coarse particles present in a sample of fine powder. For example, Fig. 7b shows a magnified plot of relative mass change for

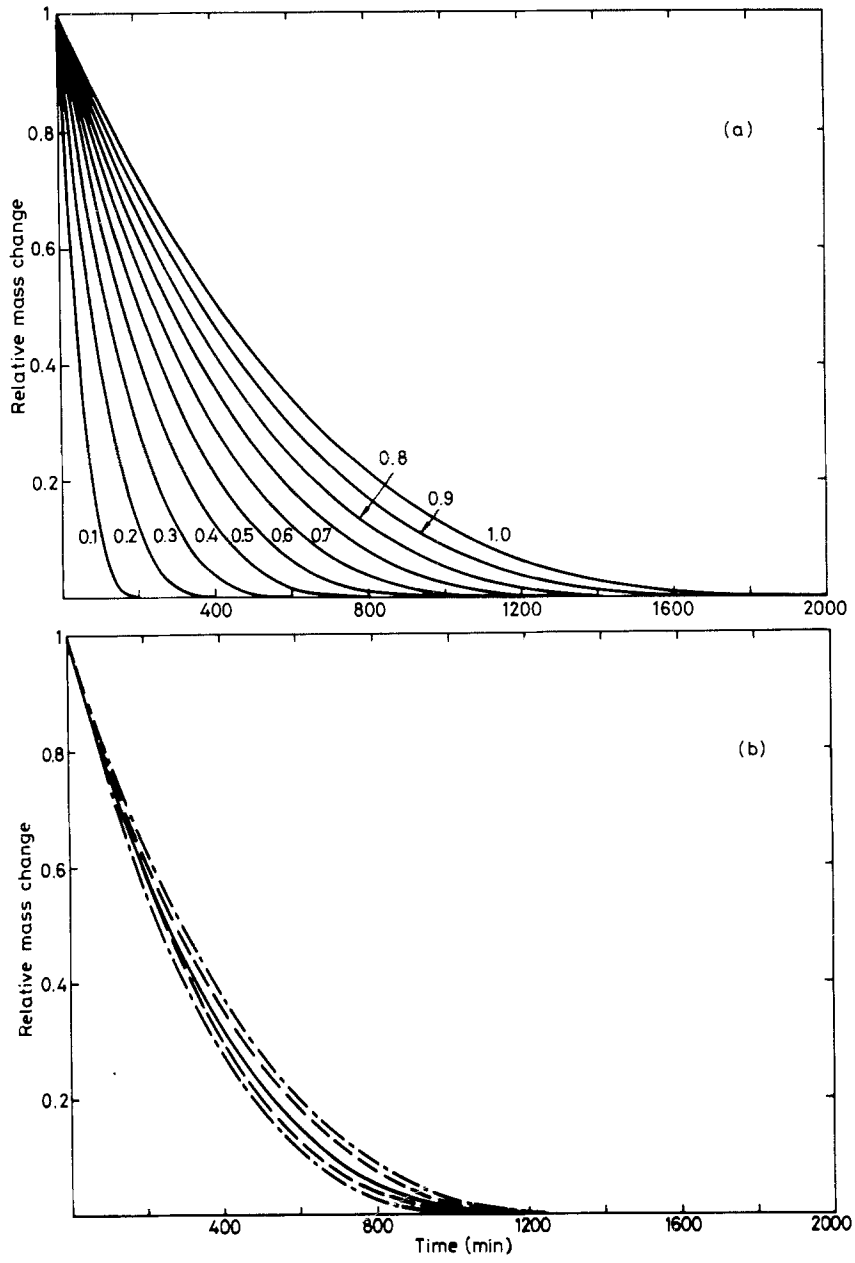

Figure 6 Theoretical plots of relative mass change showing (a) effect of particle size and (b) effects of uncertainty in temperature measurement. (---) $\pm 2°$ C, (-·-) $\pm 3°$ C.

a batch of single-sized particles of size 0.25 μm compared with that for a mixture of two particle sizes of 0.25 μm and 1 μm, with the mass fraction of the coarser particle equal to 0.01 (equivalent to a number fraction of 0.000 16) and a rate constant of 0.0005 μm min^{-1}. The separation between the two curves after a time of 500 min is equivalent to a mass fraction of 0.004. The size of the separation defines the required mass sensitivity of the thermogravimetric analyser. In the equipment used for these experiments the mass sensitivity was about 0.01 and so the example shown in Fig. 7b could not be detected. However, more modern TGA equipment can probably detect 0.0001 mass fraction changes, which is, for example, equivalent to number sensitivity of about 1 in 10^6 for two particle sizes of 1 and 10 μm.

The accuracy of the theory for describing relative mass changes of mixed powders was checked experimentally by oxidizing a mixture of equal masses of the F and C powders at 500° C. The change in mass with time is shown in Fig. 8a, and it can be seen that an attempt to fit a single cubic equation to the data by regression analysis was unsuccessful. However, a reasonable fit was obtained by using Equation 15 and this is shown in Fig. 8b. The theoretical curves were derived with Equation 15 and shown as a band indicating the uncertainty in the value of α. The values of α for the upper and lower bands were 0.000 75 and 0.000 95, respectively, and were obtained from Fig. 4. The best fit, shown in Fig. 8b, was obtained with a ratio of r_1 to r_2 of 6.5, which compares reasonably well with a ratio of about 5.5 for the ratio of particles sizes obtained from image analysis of the powder particles.

4.5. Log normal distributions

The examples quoted in the previous sections are intended to illustrate the potential of the method for analysing WC particle sizes in unknown batches, and were chosen to indicate the major limitations of the technique which are probably control of the oxidation temperature and sensitivity of measurement of mass in the gravimetric analyser. There appears to be good agreement between the theory for single-sized particles, either singly or as mixtures, and experiment. However, it is known that batches of WC powder do not comprise single-sized particles but are present as a

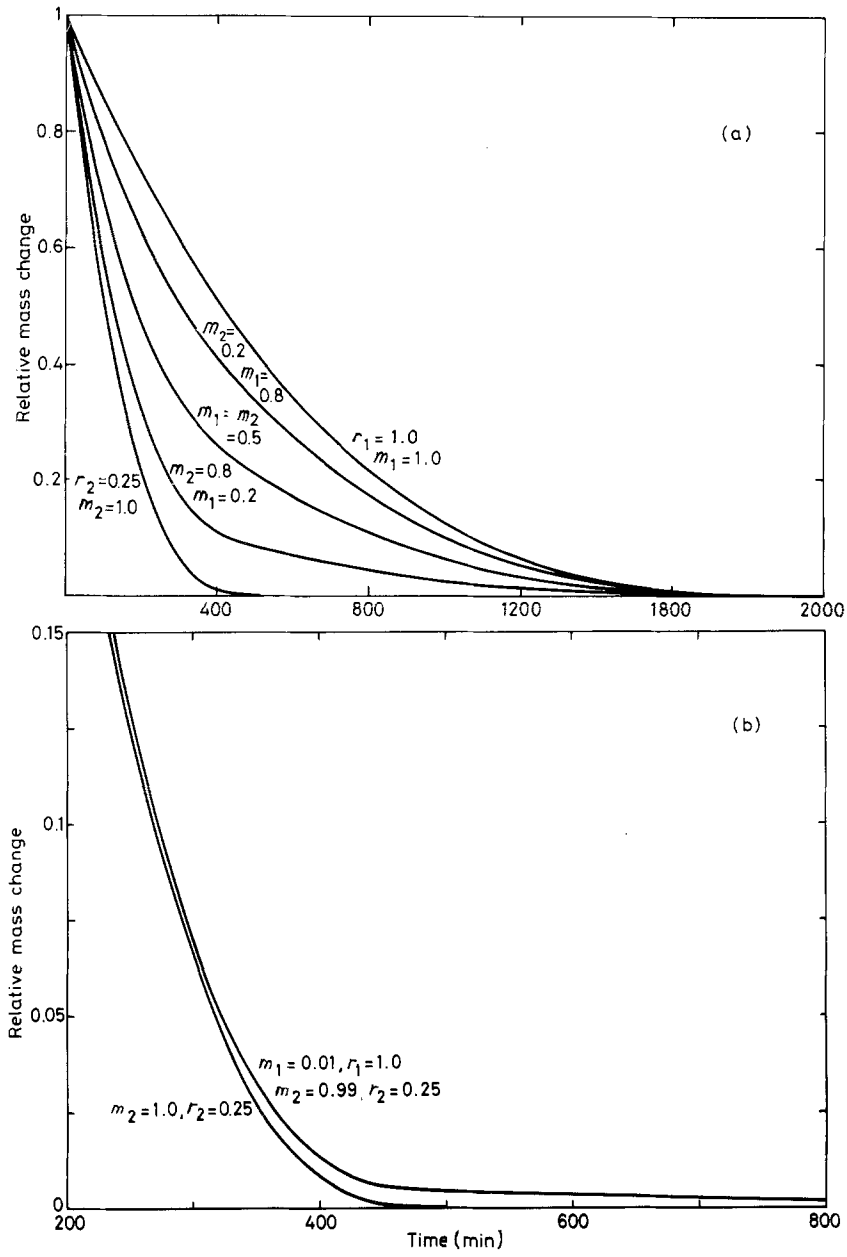

Figure 7 Theoretical plots of relative mass change showing effects of mixed particle sizes.

distribution of sizes, probably log normal. It is thus necessary to compare the experimental data with the expected change in mass for log normal distributions of powder particles with different mean values and various standard deviations. For this purpose Equations A5 and A6 (see Appendix) have been used to compute theoretical plots of relative mass change for several sets of distribution parameters. Fig. 9a shows the effects of distribution width, as defined by σ, for a particle-size distribution with a mean value of 1 μm at three values of σ (0.05, 0.2 and 0.4) compared with the plot of change in mass for particles of a single size (r = 1 μm and σ = 0). The rate constant was arbitrarily chosen to be 0.001 μm min^{-1}. The corresponding values of r for each value of σ at the limits of summation ($\pm 3\sigma$) are 1.16 and 0.86 μm, 1.82 and 0.55 μm, and 3.31 and 0.3 μm, respectively. A typical value of σ for a WC powder is probably about 0.3. Fig. 9a indicates that the effect of having a distribution of particle sizes produces a relative mass change which is equivalent to that which would be obtained with a single-sized distribution of particles with a higher mean value of particle radius. The problem of differentiating between single-sized particles and a log normal distribution of sizes is further illustrated in Fig. 9b, in which the theoretical plot for single-sized particles with r = 1.0 μm is shown alongside a plot for a log normal distribution with a mean value of r equal to 0.75 μm and a distribution width, σ, of 0.3. The curves are different in shape but it would not be possible to detect the difference with the thermogravimetric equipment used in the present work. However, the shape differences could probably be detected with more modern equipment with greater mass sensitivity and better temperature control.

5. Conclusions

The results demonstrated that a particularly good correlation was achieved between experimental measurements of the curve of mass change with time and theoretically derived results which were calculated assuming a linear oxidation rate.

The theory can also account for the effects of distributions of particle size. However, the thermogravimetric analyser used in the present work could not differentiate between the small differences in shape

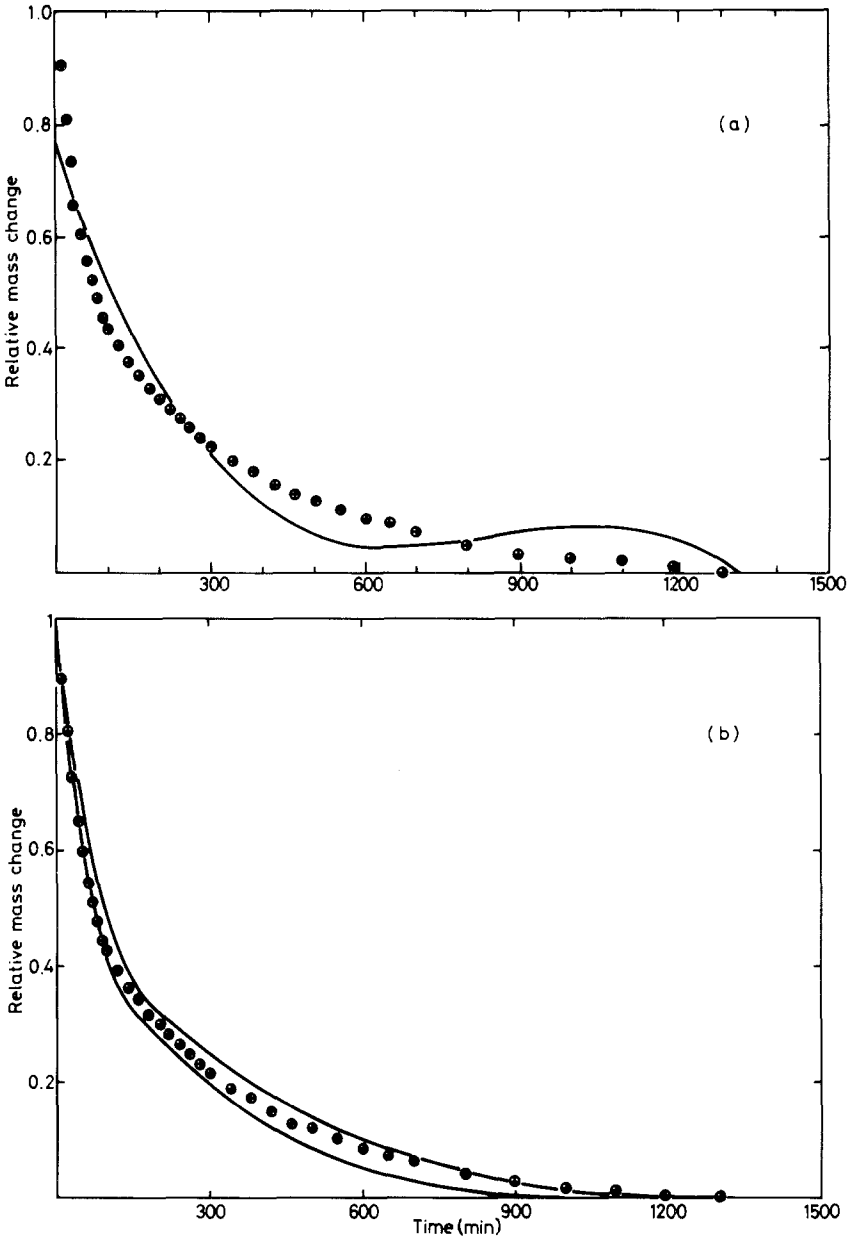

Figure 8 Comparison of theory and experiment for a powder batch with mixed particle sizes. (a) (●) Experimental data, (——) cubic regression fit; (b) (●) experimental data, (═══) theory.

of changes in mass with time from a batch of particles of single size and a batch of particles with a size which was distributed log-normally. Thus absolute particle sizes could not be deduced with confidence with the present equipment, although the technique proved its merit at discriminating between different powder batches.

The average value for the activation energy for oxidation of WC was 133 kJ mol^{-1}, and the similarity of the activation energy plots for each of the powders examined indicates that the same mechanism was probably operating in the oxidation process for each powder.

Acknowledgements

The authors would like to thank Mr G. Spriggs of Ledermann Gmbh for a supply of the ultra-fine grained WC powder, Wimet Ltd for the other WC powders, and part financial support from the EEC R&D programme in the Raw Materials Sector: Substitution and Ceramics.

Appendix: Log normal particle size distributions

For particles log-normally distributed in size [6]

$$N(r_i) = \frac{N}{(2\pi\sigma^2)^{1/2}} \frac{1}{r_i} \exp\left(-\frac{(\ln r_i - m)^2}{2\sigma^2}\right) \quad \text{(A1)}$$

where $N(r_i)$ is the initial number-size distribution of particles of WC, m is the mean and σ is the standard deviation of $\ln r_i$.

The number of particles in the range r_i to $r_i + \mathrm{d}r_i$, is therefore

$$N(r_i)\,\mathrm{d}r_i = \frac{N}{(2\pi\sigma^2)^{1/2}} \frac{1}{r_i} \exp\left[-\left(\frac{\ln r_i - m}{2\sigma^2}\right)^2\right] \mathrm{d}r_i \quad \text{(A2)}$$

Therefore from Equation 6

$$\frac{M_t}{M_1} = \int_{\alpha t}^{\infty} (r_i - \alpha t)^3 \frac{N}{(2\pi\sigma^2)^{1/2}} \frac{1}{r_i} \times \exp\left(-\frac{(\ln r_i - m)^2}{2\sigma^2}\right) \mathrm{d}r_i \left[\int_0^{\infty} r_i^3 \frac{N}{(2\pi\sigma^2)^{1/2}} \frac{1}{r_i} \times \exp\left(-\frac{(\ln r_i - m)^2}{2\sigma^2}\right) \mathrm{d}r_i\right]^{-1} \quad \text{(A3)}$$

To evaluate Equation A3 the following substitutions can be made, letting $P = \ln r_i$ and $r_i = \exp P$ so that $r_i\,\mathrm{d}P = \mathrm{d}r_i$. Thus

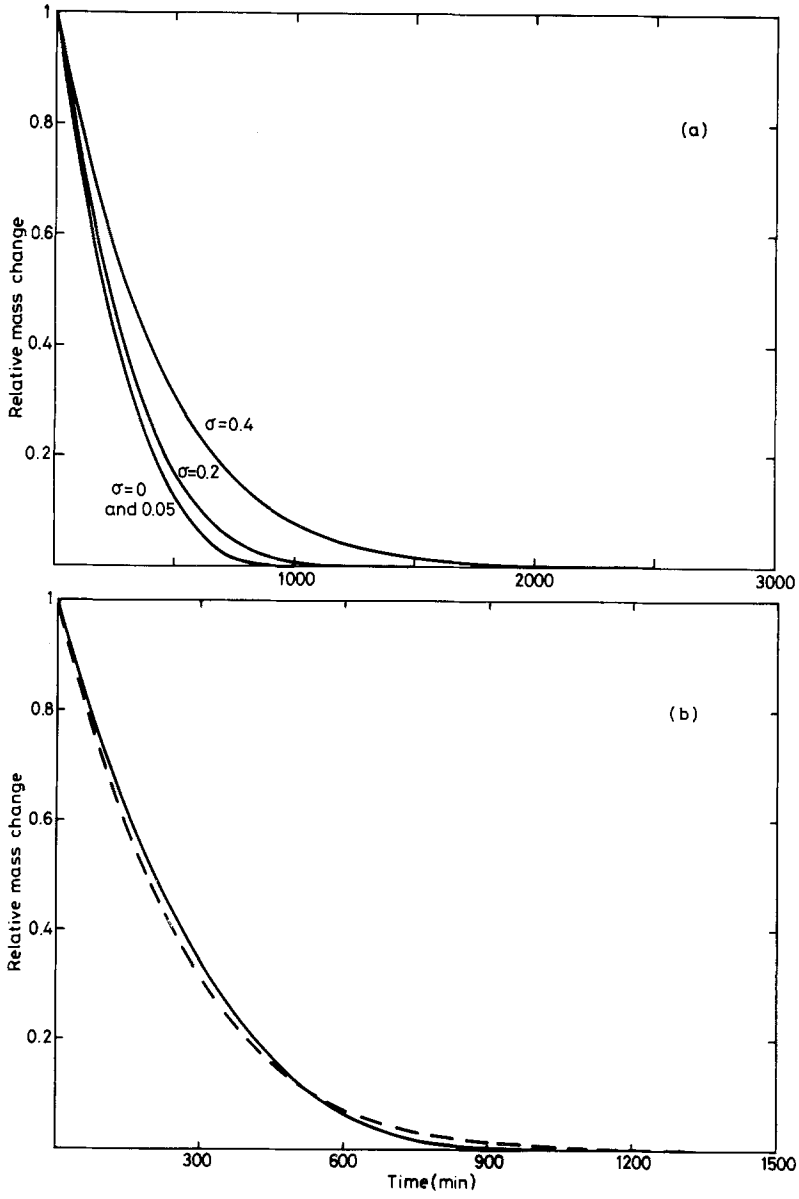

Figure 9 Theoretical plots of relative mass change for (a) log normal distributions of particle size and (b) single-sized particles compared with a log-normally distributed range of particle size; (——) $r = 1\,\mu m$ single-sized distribution, (— — —) log normal distribution with $r = 0.75\,\mu m$, $\sigma = 0.3$.

$$\frac{M_t}{M_1} = \int_{\ln \alpha t}^{\infty} (\exp P - \alpha t)^3 \exp\left(-\frac{(P-m)^2}{2\sigma^2}\right) dP \times \left[\int_0^{\infty} \exp(3P) \exp\left(-\frac{(P-m)^2}{2\sigma^2}\right) dP\right]^{-1} \quad \text{(A4)}$$

However, since 99.73% of the distribution lies between $\pm 3\sigma$ of the mean value, m, the upper and lower limits, P_2 and P_1, can be defined as

$$P_2 = m + 3\sigma \quad \text{and} \quad P_1 = m - 3\sigma$$

There are two separate stages in the oxidation process. Initially all the particles are being oxidized and the integral limits are P_1 and P_2. However, in the second stage some of the particles have completely oxidized and so the limits are from $\ln \alpha t$ to P_2. Thus, replacing the integral by a summation, for $P_1 > \ln \alpha t$

$$\frac{M_t}{M_1} = \sum_{P_1}^{P_2} (\exp P - \alpha t)^3 \exp\left(-\frac{(P-m)^2}{2\sigma^2}\right) \Delta P \times \left[\sum_{P_1}^{P_2} \exp(3P) \exp\left(-\frac{(P-m)^2}{2\sigma^2}\right) \Delta P\right]^{-1} \quad \text{(A5)}$$

and for $P_1 < \ln \alpha t < P_2$

$$\frac{M_t}{M_1} = \sum_{\ln \alpha t}^{P_2} (\exp P - \alpha t)^3 \exp\left(-\frac{(P-m)^2}{2\sigma^2}\right) \Delta P \times \left[\sum_{P_1}^{P_2} \exp(3P) \exp\left(-\frac{(P-m)^2}{2\sigma^2}\right) \Delta P\right]^{-1} \quad \text{(A6)}$$

The required accuracy can be obtained by choosing the size of the intervals ΔP.

References

1. L-C. DUFOUR and J. SIMON, *Bull. Soc. Chem. France* **9** (1969) 3643.
2. A. GIMELFARB and A. N. ZELIKMAN, *Tsvetnaya Met.* **10** (1967) 63.
3. K. SUZUKI, T. FUJIWARA and S. USUI, *J. Jpn. Soc. Powder Metall.* **23** (1976) 211.
4. R. KIEFFER and F. KOLBL, *Z. Anor. Chem.* **262** (1950) 229.
5. W. W. WEBB, J. T. NORTON and C. WAGNER, *J. Electrochem. Soc.* **103** (1956) 112.
6. G. J. HAHN and S. S. SHAPIRO, "Statistical Models in Engineering" (Wiley, New York, 1967) p. 99.

Received 11 July
and accepted 12 August 1985